

Supporting Information

Formation of a nickel-methyl species in methyl-coenzyme M reductase, an enzyme catalyzing methane formation

Na Yang,[†] Markus Reiher,[‡] Mi Wang,[†] Jeffrey Harmer,^{*§} Evert C. Duin^{*†}.

Department of Chemistry and Biochemistry, Auburn University, AL 36849, USA, Laboratory of Physical Chemistry, Department of Chemistry and Applied Biosciences, ETH-Zürich, CH-8093 Zürich, Switzerland

Index

A. Experimental Methods

B. EPR Spectroscopy

C. HYEND Spectroscopy

D. Density Functional Theory Calculations

E. Figure S1 to S8

F. Table S1 to S4

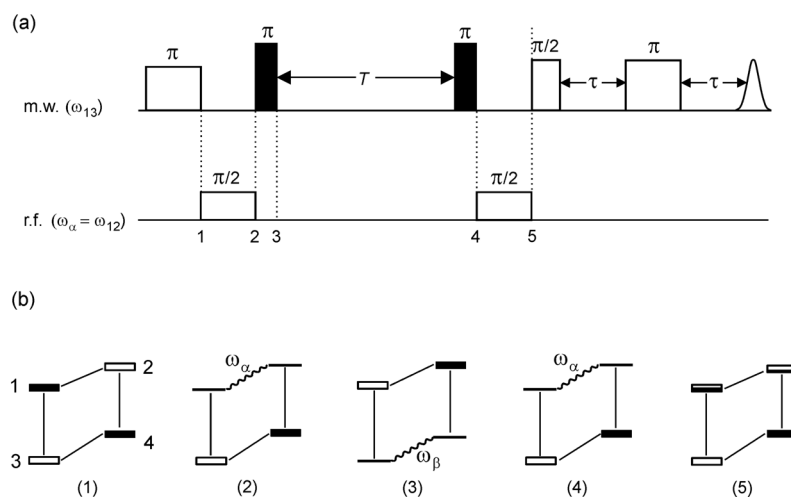
Part A. Experimental Methods. MCR was purified in the MCR_{red1c} form with 10 mM coenzyme M present in all the buffers. For this experiment, the coenzyme M was removed from the sample by extensive washing with 50 mM Tris/HCl pH 9.0 by ultrafiltration with Amicon Ultra Centrifugal Filter Devices with a 100 kDa cut off (Millipore). Complete conversion of the MCR_{red1} signal into the MCR_{BrMe} signal was achieved by incubation of 0.8 mM MCR in 50 mM Tris/HCl pH 9.0 with an approximately 50 fold excess of BrMe (saturated solution of 14 mg/ml at 25°C in 50 mM Tris/HCl pH 9.0).

Part B. EPR Spectroscopy. The continuous wave EPR experiments at Auburn were carried out at X-band (9.38 GHz) on a Bruker EMX spectrometer equipped with either a liquid nitrogen finger dewar or a Helium gas-flow cryostat from Oxford Inc. The pulse EPR experiments were carried out at X-band (9.73 GHz) and W-band (94.234 GHz) on a Bruker

E680 spectrometer equipped with a Helium gas-flow cryostat from Oxford Inc. The W-band (94.234 GHz) echo-detected EPR spectra were measured at 25 K by integrating over the echoes created with the mw pulse sequence $\pi/2-\tau-\pi-\tau$ -echo, with mw pulse lengths $t_{\pi/2} = 32$ ns, $t_{\pi} = 64$ ns, and an inter-pulse delay of $\tau = 300$ ns, 400 ns, and 500 ns. The first derivative of this spectrum was calculated numerically. The field was calibrated using the two central lines from a CaO sample containing manganese ions. The X-band Davies-ENDOR spectra were measured at 25 K with the mw pulse sequence $\pi-T-\pi/2-\tau-\pi-\tau$ -echo, with mw pulses of length $t_{\pi/2} = 28$ ns and $t_{\pi} = 56$ ns, and a $\tau = 142$ ns. A radio-frequency pulse of length 4 μ s and variable frequency ν_{ENDOR} was applied during time T . The Q-band (34.76 GHz) Davies-ENDOR spectra were measured on a home-built spectrometer at 20 K with the mw pulse sequence $\pi-T-\pi/2-\tau-\pi-\tau$ -echo, with mw pulses of length $t_{\pi/2} = 32$ ns and $t_{\pi} = 64$ ns, and a $\tau = 200$ ns. A radio-frequency pulse of length 9 μ s and variable frequency ν_{ENDOR} was applied during time T . Hyperfine correlated ENDOR (HYEND)^{S1} experiments were carried out by using the pulse sequence $\pi-\pi/2_{\text{rf}}-\pi-T-\pi-\pi/2_{\text{rf}}-\pi/2-\pi/2-\tau-\pi$ -echo, with mw pulse lengths of $t_{\pi} = 40$ ns for the preparation pulses, and $t_{\pi} = 16$ ns for the coherence transfer pulses. A selective radio frequency pulse ($\pi/2_{\text{rf}}$) of length 2 μ s and variable frequency was applied with a four-step phase cycle of the radio frequency pulse [(x,x)-(-x,x)-(x,-x)-(-x,-x)]. Time T was varied with a starting time $T_0 = 100$ ns and an increment of $\Delta T = 12$ ns. Fourier transformation along this dimension gives the hyperfine axis $\nu_{\text{HYPERFINE}}$. HYSORE experiments employed the pulse sequence $\pi/2-\tau-\pi/2-t_1-\pi-t_2-\pi/2-\tau$ -echo. Measurements were made at 25 K using the following parameters: mw pulses of lengths $t_{\pi/2} = t_{\pi} = 16$ ns, starting times 96 ns for t_1 and t_2 , and time increments $\Delta t = 16$ ns (data matrix 256×256), and a $\tau = 132$ ns. An eight-step phase cycle was used to remove unwanted echoes. The HYSORE data were processed with MATLAB 7.0 (The MathWorks, Inc.). The time traces were baseline corrected with an exponential, apodized with a Gaussian window and

zero filled. After a two-dimensional Fourier transformation absolute-value spectra were calculated. The EPR and Davies-ENDOR spectra were simulated with the program EasySpin^{S2} and the HYSCORE spectra with a program written in-house^{S3}. The orientation selection of all the X-band spectra, needed to simulated the ENDOR and HYSCORE spectra, was calculated with the g-values given and a Gaussian linewidth of 150 MHz (this simplified spin Hamiltonian accurately describes the shape of the X-band CW EPR spectrum).

Part C: HYEND Spectroscopy



Scheme S1: HYEND experiment. (a) Pulse sequence. (b) Four level energy diagrams for an $S = 1/2$, $I = 1/2$ spin system illustrating the different states obtained during the experiment.

The HYEND experiment correlates ENDOR frequencies with their corresponding hyperfine couplings. The pulse sequence is shown in Scheme S1. The nuclear frequency dimension is obtained by varying the frequency of the two selective $\pi/2$ r.f. pulses, and the hyperfine dimension by the FT of the echo modulations recorded as a function of the time T . The states attained during the experiment for an $S = 1/2$, $I = 1/2$ spin system are shown in Scheme S1. The experiment is easily understood qualitatively. We assume that the first m.w. pulse is on resonance with the allowed EPR transition (1,3) and the r.f. pulse has the frequency ω_α and is thus resonant with the nuclear transition (1,2). The first m.w. pulse inverts the polarization of transition (1,3), and the selective r.f. pulse transfers the polarization of transition (1,2) to nuclear coherence (wavy line). This coherence is immediately transferred by a non-selective m.w. π pulse to the β electron spin manifold, where it evolves with the

nuclear frequency ω_β for a time T . The second non-selective m.w. π pulse transfers the nuclear coherence back to the α manifold, where the second r.f. pulse transfers the nuclear coherence back to electron polarization, which is detected with the m.w. primary echo sequence. The two r.f. pulses must remain coherent during the sequence, and then the polarization created by the second r.f. pulse is dependent upon the phase accumulated by the nuclear coherence during the time T in the β manifold with respect to the phase of the r.f. field. This phase is given by $(\omega_\alpha + \omega_\beta)T$ (weak coupling) or $(\omega_\alpha - \omega_\beta)T$ (strong coupling). The HYEND signal as a function of T , for an isotropic hyperfine interaction with the r.f. pulses resonant with a nuclear transition, is given by

$$V_{\alpha/\beta}(T) = \pm \text{sign}(2\omega_I + A) \cos(\omega_- T) \text{ with } \omega_- = \omega_\alpha - \omega_\beta = A_S .$$

Part D: Density Functional Theory Calculations. Structure optimizations have been carried out with the Turbomole program package ^{S4} employing two different density functionals, namely the pure functional BP86 ^{S5} (in combination with the resolution-of-the-identity density fitting technique with Karlsruhe auxiliary basis sets ^{S6}) and the hybrid functional B3LYP (i.e., Becke's 3-parameter functional in combination with the LYP correlation functional ^{S7} as implemented in Turbomole). For all calculation, the valence-triple-zeta plus polarization basis set TZVP by Schäfer et al. ^{S8} was applied. While coordination energies are given below for structures optimized with both functionals, ESR spectroscopic parameters have been obtained in ADF calculations only for the BP86/TZVP structures. It is well-known that BP86 structures of transition metal complexes are in general more reliable than B3LYP structures when compared to X-ray structural data. The coordination energies have not been corrected for the basis set superposition error as the counterpoise correction turned out to be only 4 to 5 kJ/mol in test calculations on the complexes under study. The (exothermic) coordination energy of a methyl radical at 0 Kelvin amounts to -50 to -70 kJ/mol depending on the functional chosen: -68.2 kJ/mol with BP86/TZVP and to -51.9 kJ/mol with B3LYP/TZVP. These energies have been obtained for relaxed isolated fragments, i.e. for methyl radical and metal fragment cation, respectively. If

the structural relaxation is not permitted, the (intrinsic) bond energy calculated from structurally frozen, isolated fragments amounts to -170.6 kJ/mol for BP86/TZVP and to -152.8 kJ/mol for B3LYP/TZVP.

The EPR parameters, the hyperfine interactions and the g matrix, were calculated with the Amsterdam Density Functional package (ADF 2005.01). The functional RPBE with the relativistic scalar zeroth-order regular approximation (ZORA) was employed. The calculation was spin-unrestricted with a Slater-type basis set of triple- ζ quality with two polarization functions (TZ2P) with no frozen cores. For the g matrix the RPBE functional with the relativistic spin-orbit ZORA was used. In this approach spin-restricted wavefunctions are required. The basis set TZ2P was used. The coordinates for the models MCR_{BPS} and MCR_{BrMe} are given in Table S4.

Part E: Figures S1 to S8

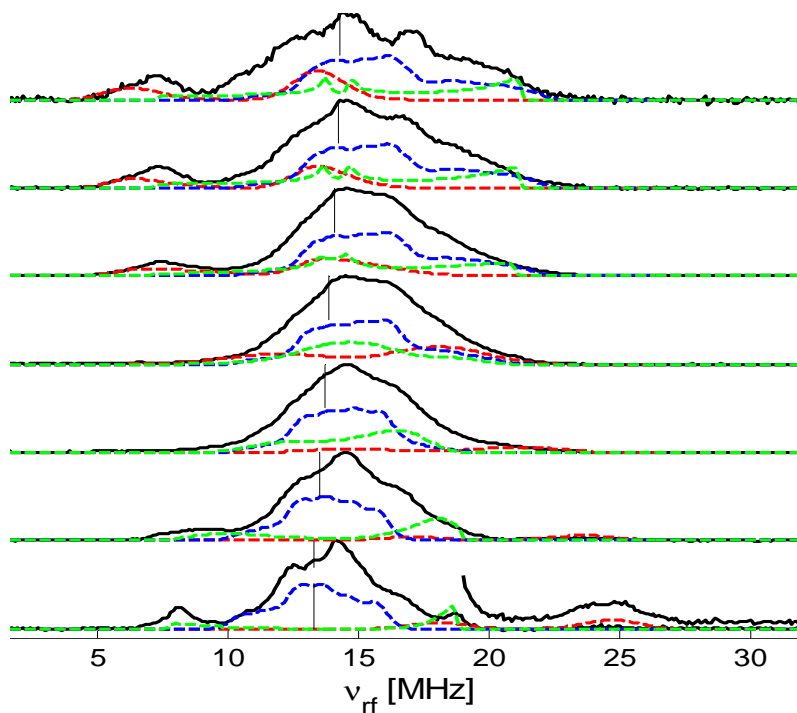


Figure S1: X-band (9.726 GHz) Davies ENDOR spectra measured at 25 K with a short π pulse of length 56 ns to attenuate signals from protons with small couplings. Field positions from bottom to top are 312.1, 316.6, 321.1, 325.6, 330.1, 333.6, 335.6 mT. Simulations: green - methyl ^1H , red line – methyl ^{13}C , and blue line – pyrrole ^{14}N .

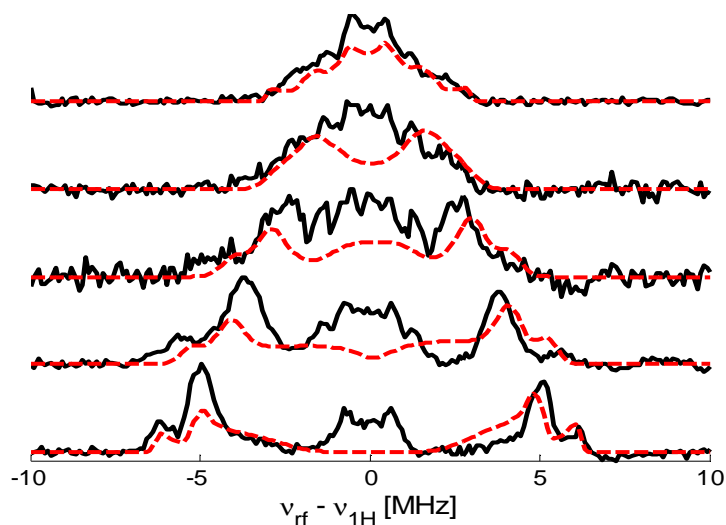


Figure S2: Q-band (34.76 GHz) Davies ENDOR spectra measured at 20 K. Experimental – solid black line, Simulation – red dotted line. Field positions from bottom to top are 1126 mT, 1140.3 mT, 1154 mT, 1169 mT, 1183 mT. Simulations include the three methyl protons with the EPR parameters given in Table S1.

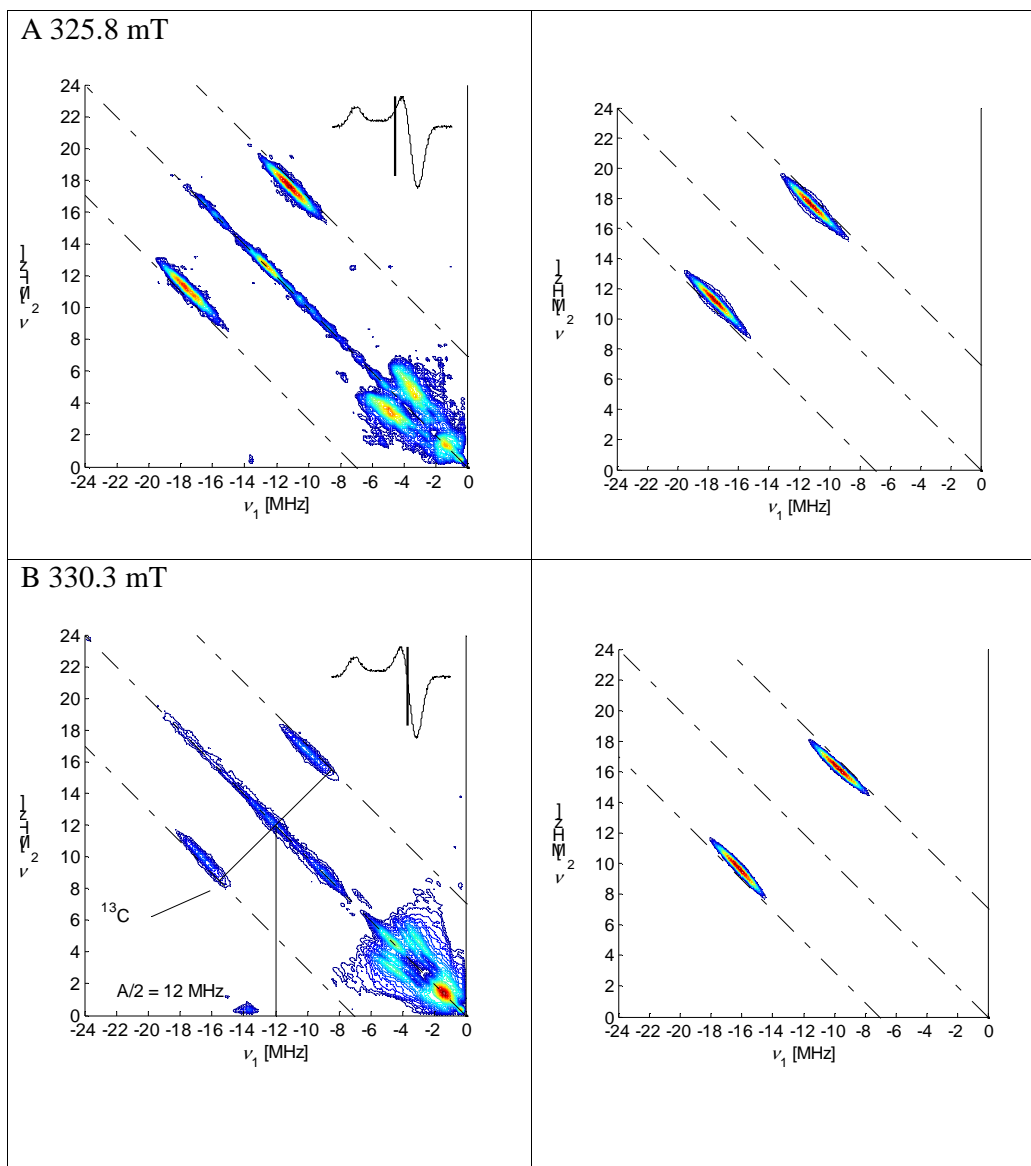


Figure S3: X-band (9.725 GHz) HYSCORE spectra of ^{13}C -MCR_{BrMe} measured at 25 K at observer position (A) 325.8 mT, (B) 330.3 mT. Right – experimental, left – simulation. In the strong coupling case ($|A| > 2|v_{13\text{C}}|$) the carbon nuclear frequencies along the principal values of the hyperfine interaction are given by $\nu = A_i/2 \pm v_{13\text{C}}$ (peaks centred at $A_i/2$ and split by $2v_{13\text{C}}$). Away from these orientations the splitting is less than $2v_{13\text{C}}$ and depends on the anisotropy of the hyperfine interaction, allowing it to be determined accurately. The low frequency features are discussed in Fig. S5.

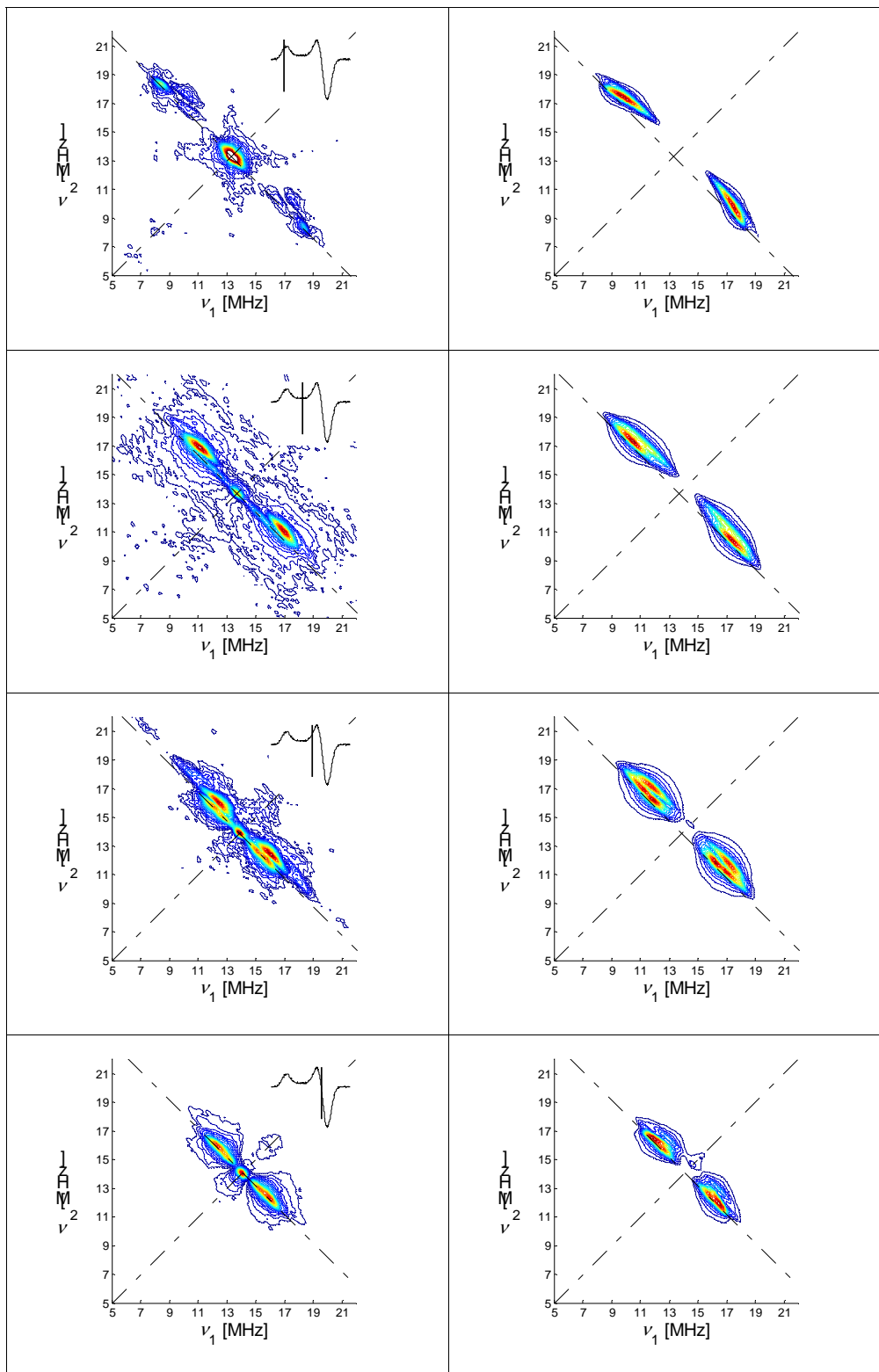


Figure S4: X-band (9.725 GHz) HYSCORE data showing the proton region of the spectrum, left – experimental, right – simulation for the three methyl nuclei using the EPR parameters given in Table S1. Field positions from top to bottom are 312.3 mT, 321.3 mT, 325.8 mT, and 330.3 mT.

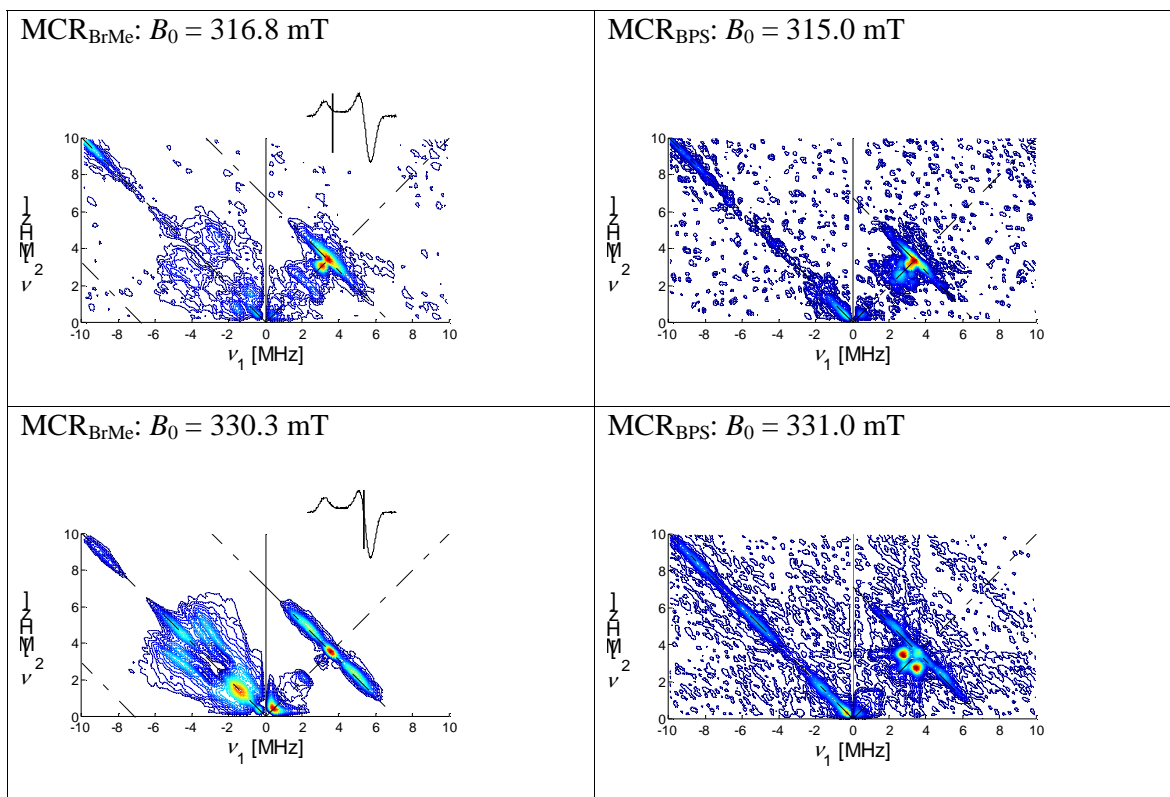


Figure S5: X-band (9.7 GHz) HYSCORE spectra showing the low frequency region. (Left) MCR_{BrMe} spectra, signals in the left-quadrant up to 7 MHz are completely absent in the corresponding MCR_{BPS} HYSCORE spectra (Right). These signals could be assigned to either the $^{79,81}Br$ anion ($I = 3/2$) or ^{14}N ($I = 1/2$) (with hyperfine couplings ranging from c.a 2-8 MHz). If these low-frequency signals are indeed from ^{14}N , then this would be evidence for a change in the distal axial ligand from $Gln^{\alpha'147}$, from O to N. Note that these signals are not from the pyrrole nitrogens of cofactor F_{430} . In the MCR_{BPS} spectra the two intense cross-peaks at c.a., (+3.5,+2.5) MHz and (+2.5,+3.5) MHz, are double-quantum peaks from a very weakly coupled nitrogen, either $Gln^{\alpha'147}$ or the lactam nitrogen of F_{430} . We also observed these peaks in MCR_{red1a} preparations (MCR in the absence of substrates). These are absent in the MCR_{BrMe} spectra. DFT calculations for MCR_{BPS} show that the $Gln^{\alpha'147}$ (coordinated via the oxygen to nickel) and the lactam nitrogen have very small hyperfine interactions (< 1 MHz), consistent with the experimental data. However, it is also reasonable to assume that the Br anion is still close to the paramagnetic centre and it may therefore produce signals in the HYSCORE spectra. Without specific labeling we therefore refrain from making an assignment. Both MCR_{BrMe} and MCR_{BPS} spectra contain ^{13}C signals, from carbon in natural abundance, along the ^{13}C anti-diagonal line in the right-quadrant.

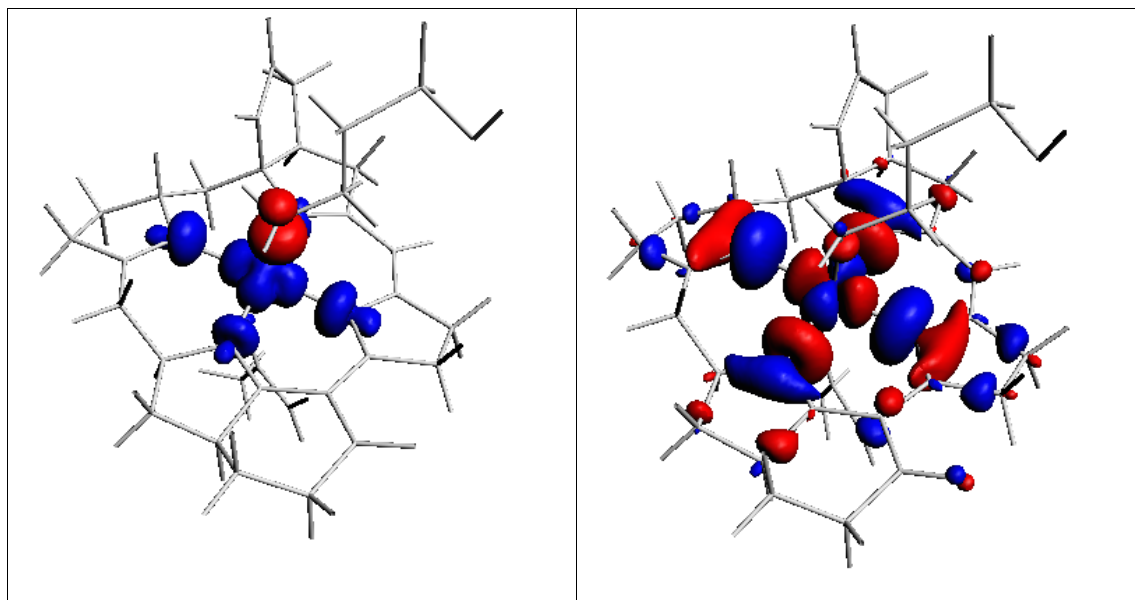


Fig S6: Spin density (level 0.003) and SOMO (level 0.03) for the MCR_{BPS} model

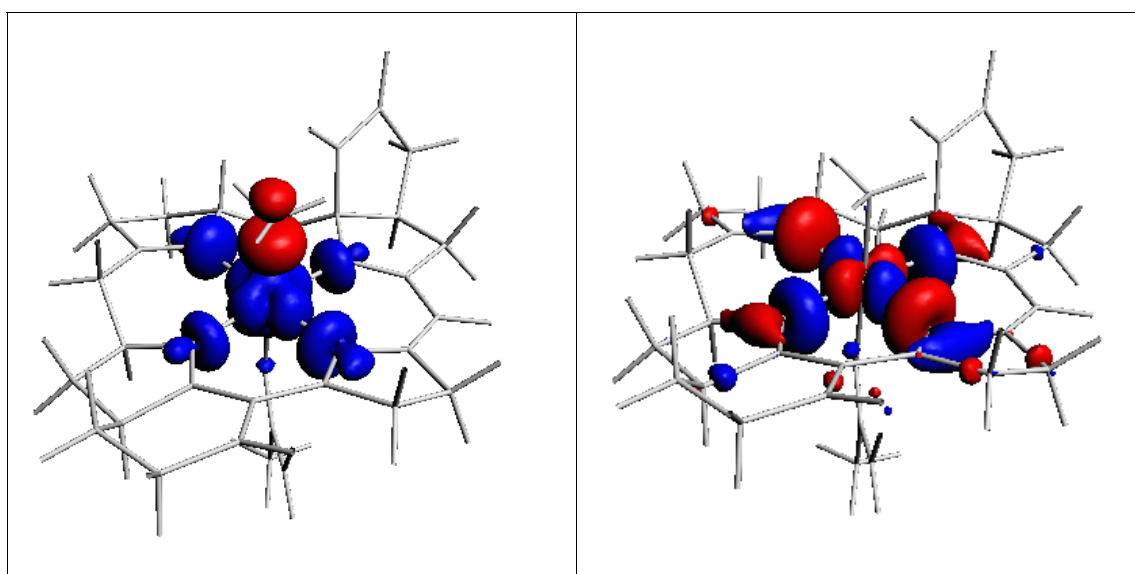


Fig S7: Spin density (level 0.003) and SOMO (level 0.03) for the MCR_{BrMe} model

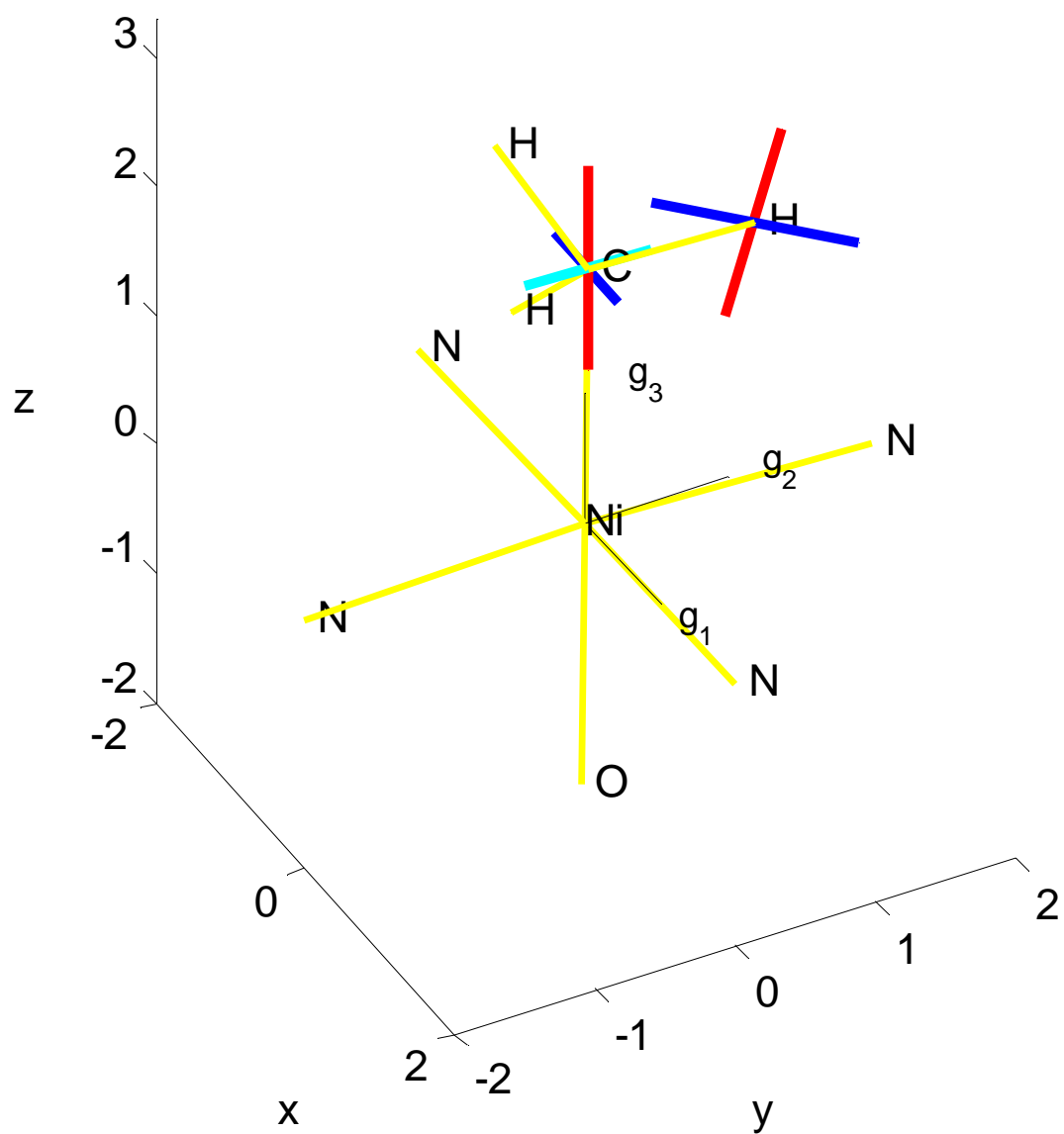


Fig S8: Orientation of the hyperfine axes of the methyl carbon and one methyl proton in the g-matrix reference frame: axis A_1 – blue, axis A_2 – cyan, axis A_3 – red.

Part F: Tables S1 to S4

Table S1: EPR parameters for the complexes MCR_{BPS} and MCR_{BrMe} . Values calculated by DFT are given in parentheses. The sign of the experimental values are given to best match the DFT result. Euler angles, *from the DFT calculation*, are given in the molecular frame defined by the coordinates in Table S4 (MCR_{BPS} model and MCR_{BrMe} model) and explain the experimental data without optimization.

Parameters for MCR_{BPS} and the DFT model complex						
	g_1	g_2	g_3	g_{iso}		$\alpha, \beta, \gamma [^\circ]$
	2.1081 (2.021)	2.1116 (2.062)	2.2193 (2.158)	2.1463 (2.082)		(-136,9,-179)
	A_1 [MHz]	A_2 [MHz]	A_3 [MHz]	A_{iso} [MHz] ^a	T_1, T_2, T_3 [MHz] ^b	
$^{13}\text{C}_\gamma$	-17.6±0.5 (-21.9)	-18.3±0.5 (-21.6)	-45.0±1 (-43.1)	-27.0 (-28.9)	(9.4,8.7,-18.0) (7.2,7.0,-14.2)	(-38,6,67)
H γ_1	-8.0 (-8.0)	-1.5 (-0.7)	13.3 (9.3)	1.3 (0.2)	-9.3,-2.8,12.0 (-8.2,-0.9,9.1)	(-135,12,-98)
H γ_2	-10.0 (-9.0)	1.0 (-1.2)	13.8 (7.7)	1.6 (-0.9)	-11.6,-0.6,12.2 (-8.2,-0.4,8.6)	(-38,19,105)
H β_1	-8.0 (-2.7)	-16.3 (-9.5)	-20.7 (-11)	-15 (-7.8)	7.0,-1.3,-5.7 (5.0,-1.8,-3.2)	(-5,135,12)
H β_2	(-1.9)	(-1.4)	(3.5)	(0.1)	(-2.0,-1.4,3.4)	(-157,32,-159)
Parameters for MCR_{BrMe} and the DFT model complex						
	g_1	g_2	g_3	g_{iso}		$\alpha, \beta, \gamma [^\circ]$
	2.093 (2.022)	2.093 (2.062)	2.216 (2.159)	2.134 (2.081)		(-136,9,-179)
	A_1 [MHz]	A_2 [MHz]	A_3 [MHz]	A_{iso} [MHz] ^a	T_1, T_2, T_3 [MHz] ^b	
$^{13}\text{C}_{\text{Me}}$	-18.0±2	-18±2	-44.0±2	-26±2	8.7,8.7,-17.3	

	(-23.7)	(-23.5)	(-42.4)	(-29.9)	(6.3,6.2,-12.5)	(109,32,-88)
¹ H _{Me}	-4.0	3.0	12.5	3.8	-7.8,-0.8,8.7	
	(-7.4)	(-0.2)	(8.0)	(0.1)	(-7.5,-0.3,7.8)	(-146,15,-113)
	-6.0	1.0	10.5	1.8	-7.8,-0.8,8.7	
	(-7.4)	(-0.9)	(7.8)	(-0.2)	(7.3,-0.7,8.0)	(-39, 9, 77)
	-6.0	1.0	10.0	1.7	-7.7,-0.7,8.3	
	(-7.2)	(-0.1)	(7.9)	(0.2)	(-7.4,-0.3,7.7)	(-7,23, 166)

$$^a A_{\text{iso}} = (A_1 + A_2 + A_3) / 3$$

$$^b (T_1, T_2, T_3) = (A_1 - A_{\text{iso}}, A_2 - A_{\text{iso}}, A_3 - A_{\text{iso}})$$

Table S2: Mulliken populations, the net spin polarization (number of electrons spin-A minus spin-B), and for each spin the atomic electron valence density (integrated) per L-value (S, P, D).

BPS	Ni	N _A	N _B	N _C	N _D	C _γ	O
Total	0.833	0.064	0.047	0.084	0.051	-0.104	0.01
S	-0.003	0.0172	0.012	0.022	0.012	-0.011	0
P	-0.009	0.0459	0.035	0.062	0.039	-0.092	0.01
D	0.845	0	0	0	0	0	0
BrMe	Ni	N _A	N _B	N _C	N _D	C _{Me}	O
Total	0.8138	0.068	0.048	0.079	0.055	-0.095	0.060
S	-0.00	0.018	0.012	0.020	0.013	-0.010	0
P	-0.010	0.049	0.036	0.058	0.041	-0.084	0.060
D	0.827	0	0	0	0	0	0

Table S3: Selected bond lengths and angles from the DFT structures.

Species	Ni-C [Å]	Ni-O [Å]	Ni-N [Å]	∠Ni-C _γ -H _γ [°] / ∠Ni-C _{Me} -H _{Me} [°]
BPS	2.01	2.19	2.23(A)	102.1
			2.03(B)	100.1
			2.09(C)	
			2.03(D)	
BrMe	1.97	2.16	2.19(A)	106.9
			2.04(B)	106.8
			2.11(C)	106.0
			2.02(D)	

Table S4: DFT Geometry optimized Coordinates for the MCR_{BPS} (left) and MCR_{BrMe} model complexes.

Model MCR _{BPS}	Model MCR _{BrMe}
C -0.289221 0.525592 -4.804659	C 0.335740 -4.193400 0.629689
C -0.062904 0.018301 -3.399096	C 0.348662 -2.765798 0.185346
O -0.148449 0.803443 -2.429484	C -0.912033 -2.102578 -0.027535
N 0.227401 -1.292552 -3.257508	C -2.184589 -2.931766 -0.148395
NI 0.296701 0.675068 -0.291386	C -2.221499 -4.072522 0.865943
N -1.312179 2.210249 -0.144553	C -0.989161 -4.951676 0.675500
C -3.076355 0.644015 0.491255	C -3.285071 -1.877426 -0.035936
C -2.568033 1.963055 0.009931	C -2.577143 -0.565179 -0.418140
C -3.478011 3.128310 -0.313546	N -1.124500 -0.812323 -0.185323
C -2.524351 4.062274 -1.075057	NI 0.243813 0.669447 -0.347169
C -1.162173 3.660787 -0.484099	C 0.552150 0.674380 1.595482
N 1.646703 2.139183 -0.658545	H 1.569939 1.041130 1.755288
C 0.068734 3.956012 -1.314626	C 1.583728 -2.135118 -0.050901
C 1.379481 3.608004 -0.591500	N 1.714847 -0.836615 -0.455455
C 2.634761 4.311045 -1.220182	C 3.042159 -0.565841 -0.720032
C 3.693607 3.203404 -1.202488	C 3.876820 -1.819737 -0.643042
C 2.902289 1.932180 -0.999342	C 2.932574 -2.820653 0.029543
N 1.427115 4.096914 0.780665	C 3.565075 0.664814 -1.015056
C 2.234333 5.201493 1.010329	C 2.897150 1.914888 -0.968126
O 2.322685 5.795203 2.069929	N 1.634001 2.128015 -0.659330
C 2.933950 5.515044 -0.315363	C 1.386073 3.597040 -0.592244
N 1.737825 -0.828447 -0.483328	C 2.613553 4.282235 -1.282365
C 3.561012 0.679227 -1.108188	C 3.681493 3.183549 -1.223505
C 3.047668 -0.558524 -0.824777	C 2.922362 5.517173 -0.427448

C	3.878206	-1.817789	-0.823755	C	2.369309	5.166151	0.959535
C	2.961507	-2.836132	-0.137727	N	1.516205	4.089169	0.778391
C	1.617221	-2.137002	-0.116548	C	0.048050	3.971783	-1.240734
N	-1.085240	-0.796824	-0.105441	C	-1.146555	3.644120	-0.371562
C	0.389729	-2.765927	0.166749	N	-1.334019	2.175008	-0.164967
C	-0.873608	-2.091916	0.022173	C	-2.591195	1.945311	0.004231
C	-2.154337	-2.913253	-0.063218	C	-3.475811	3.160251	-0.172883
C	-3.241058	-1.855120	0.115806	C	-2.517552	4.144561	-0.860676
C	-2.545043	-0.549781	-0.302903	C	-3.128813	0.607949	0.391227
C	-2.155764	-4.078330	0.923504	O	2.599127	5.714597	2.022728
C	-0.937506	-4.958419	0.657892	O	1.365532	-4.788994	0.948149
C	0.387667	-4.202968	0.579618	O	-0.164515	0.825648	-2.462354
O	1.427191	-4.806538	0.847181	C	-0.047958	0.040840	-3.430278
C	2.056512	0.658867	2.145962	N	0.338850	-1.243161	-3.285433
C	2.243931	1.289590	3.532992	C	-0.339817	0.521085	-4.832477
C	0.614305	0.759940	1.690836	H	2.916132	-3.816559	-0.425327
S	4.028193	1.457826	3.951778	H	3.188193	-2.997549	1.084961
O	4.455916	-0.173837	4.023579	H	-1.268981	1.103236	-4.833541
O	4.723744	2.042908	2.785422	H	-0.421868	-0.296713	-5.559350
O	4.174294	2.012215	5.317111	H	0.470767	1.192137	-5.151365
H	2.908963	-3.813589	-0.629207	H	0.468054	-1.849586	-4.087537
H	3.274292	-3.057701	0.893549	H	0.641251	-1.566822	-2.367398
H	-1.199300	1.137094	-4.828114	H	-2.915777	0.434583	1.460821
H	-0.374266	-0.278074	-5.546695	H	-4.224036	0.611573	0.288719
H	0.552413	1.175143	-5.084566	H	-4.385765	2.927052	-0.743936
H	0.339249	-1.897733	-4.063167	H	-3.808242	3.520623	0.817568
H	0.476258	-1.652102	-2.337582	H	-2.586091	4.044299	-1.954802

H -2.812083 0.515464 1.554806	H -2.698334 5.194227 -0.598794
H -4.174664 0.632442 0.436266	H -0.963150 4.069509 0.632837
H -4.367015 2.814129 -0.878731	H -0.034581 3.465458 -2.213626
H -3.844989 3.580507 0.625976	H 0.052302 5.058699 -1.420297
H -2.549009 3.839700 -2.152989	H 2.367579 4.531663 -2.323136
H -2.745603 5.127585 -0.936589	H 4.287344 3.107038 -2.137355
H -1.050073 4.185139 0.483590	H 1.029975 3.681859 1.572124
H 0.031149 3.409076 -2.267386	H 3.989307 5.762813 -0.362002
H 0.078405 5.034733 -1.538007	H 2.404570 6.418937 -0.788702
H 2.409088 4.608981 -2.252630	H 4.632118 0.702699 -1.237198
H 4.305035 3.162513 -2.114776	H 4.154173 -2.145782 -1.658975
H 0.783070 3.793169 1.504609	H 4.812673 -1.654947 -0.094014
H 4.003704 5.690322 -0.144781	H -2.179337 -3.371824 -1.164641
H 2.513205 6.452987 -0.706823	H -4.154862 -2.085543 -0.671570
H 4.619473 0.721123 -1.366432	H -3.636769 -1.818757 1.006639
H 4.110745 -2.114699 -1.859493	H -2.703039 -0.343872 -1.492741
H 4.836768 -1.670485 -0.310059	H -2.238310 -3.652480 1.885525
H -2.194986 -3.328964 -1.089284	H -3.143117 -4.661383 0.747404
H -4.146626 -2.055103 -0.471029	H -0.892478 -5.714741 1.458821
H -3.532612 -1.796395 1.176985	H -1.064981 -5.500065 -0.281432
H -2.696669 -0.352531 -1.379161	H 4.385111 3.341735 -0.388617
H -2.127328 -3.684070 1.953279	H 0.428805 -0.357002 1.937796
H -3.085258 -4.658945 0.828777	H -0.208348 1.337131 2.020843
H -0.813220 -5.745637 1.413062	
H -1.057138 -5.477371 -0.310992	
H 2.728252 1.187455 1.459837	
H 2.380996 -0.388588 2.180337	

H	1.889702	2.330213	3.574140
H	1.792284	0.720640	4.355621
H	4.860365	-0.299483	4.907654
H	4.390152	3.313958	-0.353833
H	-0.019117	-0.054320	2.059700
H	0.153335	1.728922	1.918537

References

^{S1} Jeschke, G.; Schweiger, A. *Chem. Phys. Lett.* **1995**, *246*, 431.

^{S2} see <http://www.esr.ethz.ch>

^{S3} Madi, Z.; Van Doorslaer, S.; Schweiger, A. *J. Magn. Reson.* **2002**, *154*, 181-191.

^{S4} Ahlrichs, R.; Bär, M.; Häser, M.; Horn, H.; Kölmel, C. *Chem. Phys. Lett.*, **1989**, *162*, 165-169.

^{S5} Becke, A.D. *Phys. Rev. A*, **1988**, *38*, 3098-3100; Perdew, J. P. *Phys. Rev. B*, **1986**, *33*, 8822-8824.

^{S6} <ftp://ftp.chemie.uni-karlsruhe.de/pub/jbasen>

^{S7} Becke, A.D. *J. Chem. Phys.*, **1993**, *98*, 5648-5652; Lee, C.; Yang, W.; Parr, R.G. *Phys. Rev. B*, **1988**, *37*, 785-789.

^{S8} Schäfer, A.; Huber, C.; Ahlrichs, R. *J. Chem. Phys.*, **1994**, *100*, 5829.